Anal. Chem. **2002,** *74,* 886−894

Aluminum Surface Corrosion and the Mechanism of Inhibitors Using pH and Metal Ion Selective Imaging Fiber Bundles

Sabine Szunerits and David R. Walt*

The Max Tishler Laboratory for Organic Chemistry, Department of Chemistry, Tufts University, Medford, Massachusetts 02155

The localized corrosion behavior of a galvanic aluminum copper couple was investigated by in situ fluorescence imaging with a fiber-optic imaging sensor. Three different, but complementary methods were used for visualizing remote corrosion sites, mapping the topography of the metal surface, and measuring local chemical concentrations of H^+, OH^-, and Al^{3+}. The first method is based on a pH-sensitive imaging fiber, where the fluorescent dye SNAFL was covalently attached to the fiber's distal end. Fluorescence images were acquired as a function of time at different areas of the galvanic couple. In a second method, the fluorescent dye morin was immobilized on the fiber-optic imaging sensor, which allowed the in situ localization of corrosion processes on pure aluminum to be visualized over time by monitoring the release of Al^{3+}. The development of fluorescence on the aluminum surface defined the areas associated with the anodic dissolution of aluminum. We also investigated the inhibition of corrosion of pure aluminum by $CeCl_3$ and 8-hydroxyquinoline. The decrease in current, the decrease in the number of active sites on the aluminum surface, and the faster surface passivation are all consistent indications that cerium chloride and 8-hydroxyquinoline inhibit corrosion effectively. From the number and extent of corrosion sites and the release of aluminum ions monitored with the fiber, it was shown that 8-hydroxyquinoline is a more effective inhibitor than cerium chloride.

The corrosion behavior of aluminum and its alloys has been studied in numerous ways, primarily based on potentiostatic experiments, to determine the critical pitting potential.[1−3] These methods are limited in their ability to visualize the surface during the corrosion process and monitor its progression. Assessment of spatial variations in electrochemical activity in situ requires techniques that respond to some properties of the surface or the solution proximal to the surface with a high degree of spatial resolution. A variety of techniques have been used to scan a probe over the sample surface and to monitor the response to provide spatial resolution in the micrometer range.[4−11] Optical methods have been used widely to spatially resolve electrochemical activity, including photoelectrochemical measurements, electrochemiluminescence imaging, and fluorescence imaging of electrode−solution interfacial processes.[12−21] One approach to fluorescence imaging is to electrochemically generate a species that is either itself fluorescent or that reacts in the interfacial region with a fluorescent agent added to the solution. Fluorescence imaging (FI)[17−21] has proven particularly useful for spatially resolving the electrochemical activity at solid electrodes. Engstrom[17] used FI to image cathodic centers in copper−aluminum corrosion cells and demonstrated that the increase in fluorescence at copper is attributed to the production of hydroxide ions while the decrease at the aluminum electrode is attributed to the production of hydrogen ions through the hydrolysis of aluminum ions. Smyrl[19,20] investigated corrosion initiation on Al2024 via fluorescence and near-field scanning optical microscopy. For characterizing the initial state of pitting in situ, high-resolution microscopy techniques such as FI are needed to reveal the nature of the surface chemistry along with surface topography around the active sites. A variety of other techniques have been used to observe localized corrosion including near-field scanning optical microscopy (NSOM),[19] atomic

(1) Suter, T.; Alkire, R. C. Critical factors in localized corrosion III. In *Proceedings, of the Electrochemical Society*; Kelly, R. G., Frankel, P. M., Natishan, Newmann, R. C., Eds.; The Electrochemical Society: Pennington, NJ, 1998: Vol. PV 98−17, pp 118−129.
(2) Guillaumin, V.; Mankowski, G. *Corros. Sci.* **1999**, *41*, 421.
(3) Blanc, C.; Lavelle, B.; Mankowski, G. *Corros. Sci.* **1997**, *39*, 495.
(4) Isaacs, H. S.; Kissel, G. *J. Electrochem. Soc.* **1972**, *119*, 13.
(5) Isaacs, H. S.; Kendig, M. W. *Corrosion* **1980**, *36*, 269.
(6) Engstrom, R. C. *Anal. Chem.* **1984**, *56*, 890.
(7) Engstrom, R. C.; Weber, M.; Werth, J. *Anal. Chem.* **1985**, *57*, 844.
(8) Engstrom, R. C.; Weber, M.; Wunder, D. J.; Burgess, R.; Winquist, S. *Anal. Chem.* **1986**, *58*, 844.
(9) Bard, A. J.; Denuault, G.; Lee, C.; Mandler, D.; Wipf, D. O. *Acc. Chem. Res.* **1990**, *23*, 357.
(10) Liu, H. Y.; Fan, R. R.; Lin, C. W.; Bard, A. J. *J. Am. Chem. Soc.* **1986**, *108*, 3838.
(11) Panova, A. A.; Pantano, P.; Walt, D. R. *Anal. Chem.* **1997**, *69*, 1635.
(12) Rubinstin, I. J. *Appl. Electrochem.* **1983**, *13*, 689.
(13) Butler, M. A. *J. Electrochem. Soc.* **1984**, *131*, 2185.
(14) Engstrom, R. C.; Johnson, K. H.; DesJarlais, S. *Anal. Chem.* **1987**, 59, 670.
(15) Pharr, C. M.; Engstrom, R. C.; Klancke, J.; Unzelman, P. L. *Electroanalysis* **1990**, *2*, 217.
(16) Vitt, J. E.; Johnson, D. C.; Engstrom, R. C. *J. Electrochem. Soc.* **1991**, *128*, 1637.
(17) Engstrom, R. C.; Ghaffari, S.; Qu, H. *Anal. Chem.* **1992**, *64*, 2525.
(18) Patterson, M. L.; Allen, C. S. *Anal. Chem.* **1985**, *57*, 2751.
(19) Büchler, M.; Kerimo, J.; Guillaume, F.; Smyrl, H. W. *J. Electrochem. Soc.* **2000**, *147*, 3691.
(20) Büchler, M.; Watari, T.; Guillaume, F.; Smyrl, H. W. *Corros. Sci.* **2000**, *42*, 1661.
(21) Schmutz, P.; Frankel, G. S. *J. Electrochem. Soc.* **1998**, *145*, 2295.

10.1021/ac0108257 CCC: $22.00
Published on Web 01/17/2002

force microscopy (AFM),[20−23] confocal laser scanning microscopy (CLSM)[24,25] and scanning electrochemical microscopy (SEM).[26]

In our laboratory, fluorescence imaging to investigate localized corrosion[11] has been performed by optical imaging fibers to which a pH-sensitive dye, SNAFL, was covalently bound to the distal end of the fiber surface. In this paper, we present further results with these pH-sensitive fibers and describe the use of an aluminum ion-sensitive optical fiber to obtain further details about what is occurring on the metal surfaces under different conditions. The advantage of covalently attaching fluorescent dyes to the fiber's distal end is that the dyes do not have to be dissolved in solution where they may alter the chemistry being observed.

These dye-modified fibers were used further to investigate the effect of inhibitors on the corrosion of an aluminum/copper galvanic couple. Aluminum dissolution can be prevented by the action of adsorptive inhibitors, which prevent the adsorption of aggressive ions or facilitate the formation of oxide films on the metal surface. There are a variety of different materials for inhibiting aluminum dissolution in neutral and slightly acidic media. Chromium compounds have been used extensively to inhibit corrosion of aluminum alloys but, due to chromium's toxicity, severe restrictions have been imposed on its use.[27,28] The organic compound 8-hydroxyquinoline has proven to be an effective inhibitor of corrosion as it forms a chelate with dissolved aluminum ions.[29] Lanthanide salts, such as cerium salts,[30−34] have also been found to be effective in reducing the corrosion rate of aluminum by inhibiting the cathodic reaction via formation of a cerium-rich film over the cathodic copper surface.[32−34]

In this work, we fabricated an aluminum/copper galvanic couple and investigated separately the anodic and cathodic sites with modified optical fiber imaging bundles. This couple was designed to mimic aluminum-containing intermetallics resulting from copper alloying. To investigate the inhibition effects of cerium chloride and 8-hydroxyquinoline, we make use of the fact that acidification takes place close to the electrode surface when corrosion is initiated. A pH-sensitive imaging fiber allowed concurrent viewing of the sample while measuring ions at the surface.[11,35] In this combined imaging and sensing approach, a pH-sensitive fluorescent dye is immobilized on the distal end of a imaging fiber, with a surface area of 0.35 mm^2, in such a way that the fiber's imaging capability was not affected. To analyze larger surfaces than the imaging fiber covered, we employed a micromanipulator to scan the fiber over the aluminum surface to obtain a full chemical image.

Scheme 1. Formation of the Aluminum Chelate of Morin (**1**)

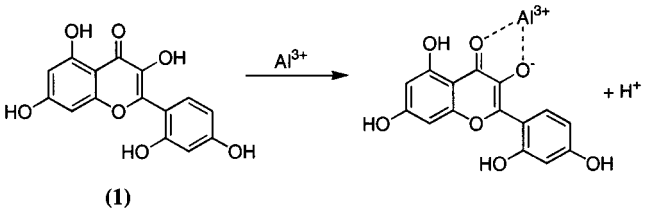

(1)

Chemical features were further investigated with the use of morin, a fluorescent dye, in solution. Morin forms a highly fluorescent complex with Al^{3+} (Scheme 1), which could be imaged with the optical fiber bundle to localize regions of corrosion on the surface of the metal. Areas of high fluorescence associated with an aluminum−morin chelate are due to localized surface corrosion. The fluorescent features represent precipitated corrosion products.

The third investigation tool was a sensor for Al^{3+} based on immobilized morin. In this case, morin was covalently linked to a polymer layer on the end of the imaging fiber. Morin was observed to bind Al^{3+}, and the imaging fiber could be regenerated by dipping it into a solution of EDTA to dissociate the complex. Morin was used in combination with the pH-sensitive fiber to reveal both temporal and spatial details of the chemistry at individual reaction sites.

EXPERIMENTAL SECTION

Materials. Aluminum (1.5-mm diameter) and copper (500-μm diameter) wire were purchased from Goodfellow Cambridge Ltd. Cerium chloride heptahydrate, morin, sodium chloride, 8-hydroxyquinoline, triethylenetetramine, (3-aminopropyl)triethoxysilane, and THF were purchased from Aldrich and used without further purification. 4-(2-Hydroxyethyl)-1-piperazineethanesulfonic acid (HEPES), acrylamide, *N*-acryloxysuccinimide aluminum ammonium sulfate dodecyl hydrate, phosphate buffer, Tris-EDTA buffer, and glycerol were obtained from Sigma Chemical Co. The 350-μm-diameter imaging fiber comprised about 6000 optical fibers, each with a diameter of 2−3 μm, obtained from Sumitomo Electric Industries (Torrance, CA). 5-(and-6-)carboxysuccinimidyl ester (SNAFL-SE) was obtained from Molecular Probes. The epoxy resin used was Araldite AW 136 supplied by Ciba-Geigy.

Instrumentation. An aluminum wire (diameter, 1.5 mm) and a copper wire (diameter, 500 μm) were separately incorporated into epoxy resin, polished at one end to a 0.3-μm finish and placed face upward into a rubber vial of 5-mL volume. The potentiostat used was a PGSTAT 30 Autolab (Eco Chemie). The potential applied between the copper and the aluminum electrode was +0.4 V/Cu.

The instrumental setup for imaging and fluorescence measurements has been described in detail previously.[36] The excitation wavelength for SNAFL was 490 nm, and the emission ratio was measured at 540/650 nm. The pK_a for SNAFL is 7.8 and shows sigmoidal pH dependence with the most sensitive region being between pH 6.2 and 8.6. For morin, the emission wavelength was set at 430 nm and the emission was monitored at 500 nm.

(22) Kowal, K.; DeLuccia, J.; Josefowicz, J. Y.; Laird, C.; Farrington, G. C. *J. Electrochem. Soc.* **1996**, *143*, 2471.
(23) Rynders, R.; Paik, C.; Ke, P.; Alkire, R. *J. Electrochem. Soc.* **1994**, *141*, 1439.
(24) Aladan, M. A.; Smyrl, H. W. *J. Electrochem. Soc.* **1997**, *144*, 1282.
(25) Alodan, M. A.;, Smyrl, H. W. *J. Electrochem. Soc.* **1998**, *145*, 1571.
(26) Chen. G.; Gao, M.; Wei R. *Corros. Sci.* **1996**, *52*, 1.
(27) Brett, C. M. A.; Gomes, I. A. R.; Martins, J. P. S. *Corros. Sci.* **1994**, *36*, 915.
(28) Maji, K. D.; Singh, I. *Anti-Corros. Methods Mater.* **1982**, *29*, 8.
(29) Garrigues, L.; Pebere, N.; Dabosi, F. *Electrochim. Acta* **1996**, *41*, 1209.
(30) Bethencourt, M.; Botana, F. J.; Calvino, J. J.; Marcos, M.; Rodríguez-Chacón, M. A. *Corros. Sci.* **1998**, *40*, 1803.
(31) Aldykewicz, A. J.; Isaacs, H. S.; Davenport, A. J. *J. Electrochem. Soc.* **1995**, *142*, 3342.
(32) Hinten, B. R. W.; Arnott, D. R.; Ryan N. E. *Met. Forum* **1984**, *7* (4), 11.
(33) Hinten, B. R. W.; Arnott, D. R.; Ryan N. E. *Corros. Australas.* **1985**, *10* (3), 12.
(34) Hinten, B. R. W.; Arnott, D. R.; Ryan N. E. *Met. Forum* **1986**, *9* (3), 162.
(35) Khan, S. S.; Jin, E. S.; Pantano, P. *Anal. Chim. Acta* **2000**, *404*, 213.
(36) Bronk, K. S.; Michael, K. L.; Pantano, P.; Walt, D. R. *Anal. Chem.* **1995**, *67*, 2750.

Excitation light from a 75-W xenon arc lamp was transmitted through the fiber's proximal face to the distal face where it illuminated the sensing layer. The fluorescence returning through the imaging fiber was transmitted through a dichroic mirror and detected by a CCD camera (PXL-37, Photometric, Tucson, AZ).

The distal end of an imaging fiber (diameter, 350 μm) was placed 10 μm above the surface of the metal with the use of a three-axis micromanipulator MMO-203 (Narishige Scientific Instruments Lab., Tokyo, Japan). Positioning was accomplished by first touching the surface with the fiber and then withdrawing it. Once positioned, fluorescence images were acquired through the imaging fiber as a function of time, with a typical acquisition time of 300−500 ms. The solutions investigated were NaCl (0.1 M) in phosphate buffer, pH 7.0 (0.1 mM), and NaCl (0.1 M) in phosphate buffer, pH 7.0, with either $CeCl_3$ (3.0 mM) or 8-hydroxyquinoline (3.0 mM) present.

Fabrication of a pH and an Aluminum Sensor. The polished fiber was silanized in a 10 mM solution of (3-aminopropyl)triethoxysilane in acetone. The imaging fiber's distal end was then further modified with a thin layer of poly(acrylamide-*co*-*N*-acryloxysuccinimide) (PAN),[37] to which the pH-sensitive fluorescent dye, SNAFL-SE, was covalently attached as described previously.[11]

A stable aluminum sensor was constructed by covalently attaching morin (**1**) to the distal end of an imaging fiber, previously modified with (3-aminopropyl)triethoxysilane and a PAN layer. Morin was immobilized using cyanuric chloride according to a previous procedure.[38−41] The PAN-modified fibers were left in a solution of morin (8.0 mM) and cyanuric chloride (0.14 M) in acetone for 1 h. The modified fiber was then washed by dipping it into acetone and water. Morin was also immobilized as its Al^{3+} complex as this should prevent the functional groups involved in the complexation from reacting with cyanuric chloride. The uncomplexed morin gave higher intensities than the morin bound as its Al^{3+} complex, and consequently, the uncomplexed form was used for immobilization. Before use, the sensor's response to Al^{3+} solutions (0.5−40 mM in phosphate buffer, pH 7) was tested and the sensor was calibrated. After the fiber responded to Al^{3+}, the Al^{3+} bound to the morin was stripped off by immersing the fiber in a solution of EDTA (0.1 M pH 7) and then washing with water.

RESULTS AND DISCUSSION

Corrosion in 0.1 M NaCl. pH-Sensitive Fiber. When a fresh aluminum surface is exposed to air, it is immediately covered with a protective amorphous oxide coating. Anions such as SO_4^{2-} and Cl^- deposited on the oxide layer may react with the oxide to form water-soluble salts. When chloride ions are present, migration of Cl^- into the oxide layer is believed to take place, thereby lowering the resistance to outward migration of Al^{3+} and initiating pitting.[42] The first step of aluminum corrosion, therefore, is attack of the oxide layer by chloride ions leaving a bare aluminum surface. In the propagation stage, aluminum is dissolved anodically to Al^{3+} ions within the pit (reaction 1). In the case of a galvanostatic couple, the cathodic reaction takes place on the copper surface and consists of the reduction of oxygen or water to hydroxide ions (reactions 3 and 4).

1. Anode

$$Al \rightarrow Al^{3+} + 3e^- \quad (1)$$

$$Al^{3+} + H_2O \rightarrow Al(OH)^{2+} + H^+ \quad (2a)$$

$$Al(OH)^{2+} + H_2O \rightarrow Al(OH)_2^{+} + H^+ \quad (2b)$$

$$Al(OH)_2^{+} + H_2O \rightarrow Al(OH)_3 + H^+ \quad (2c)$$

$$Al(OH)_3 + H_2O \rightarrow Al(OH)_4^{-} + H^+ \quad (2d)$$

$$xAl^{3+} + yH_2O \rightarrow Al_x(OH)_y^{3x-y} + yH^+ \quad (2e)$$

2. Cathode

$$2H_2O + 2e^- \rightarrow 2OH^- + H_2 \quad (3)$$

$$O_2 + H_2O + 4e^- \rightarrow 4OH^- \quad (4)$$

The chemistry of Al^{3+} in aqueous solution is complex and is dominated by the interaction of Al^{3+} with water to form hydrolytic species (reactions 2a−d). The solubility of aluminum and the oxyhydroxy complexes formed depend on the solution pH. The concentration of aluminum in solution varies significantly as the solution pH moves from acidic to basic pH, where Al^{3+} and $Al(OH)_4$ are the predominant stable species, respectively. In concentrated solutions at intermediate pH values, polynuclear aluminum species with x values up to 13 have been reported, although in natural waters, particularly at elevated temperatures and at low aluminum concentrations, only monomeric $Al(OH)_y^{3-y}$ species ($y = 0-4$) are important.[43−47] Independent of the complex formed, acidic conditions are created within the pit during the hydrolysis of the Al^{3+} ions and a cap of $Al(OH)_3$ or Al_2O_3 is formed over its mouth that finally blocks further aluminum dissolution.

For the present discussion, the particular nature of the aluminum species formed during hydrolysis is not critical and reaction 2e represents the general reaction scheme. In the formation of all the hydrolysis products, hydrogen ions are released and acidification is observed in the proximity of the aluminum surface as monitored in situ with the fiber (reactions 2a−d).

Figure 1 shows the fluorescence intensity of the immobilized pH-sensitive dye SNAFL-SE when the imaging fiber was brought into contact with the aluminum anode or the copper cathode of the galvanic couple and a constant anodic potential of 0.4 V was applied. The potential of 0.4 V/Cu was chosen in order to minimize convection due to H_2 gas evolution.[17] In the images, a decrease

(37) Pollak, A.; Blumenfeld, H.; Wax, M.; Baughn, R. L.; Whitesides, G. M. *J. Am. Chem. Soc.* **1980**, *102*, 6324.
(38) Saarl, L. A.; Seitz, W. R. *Anal. Chem.* **1983**, *55*, 667.
(39) Narayanaswamy, R.; Ahmad, M. *Sci. Total Environ.* **1995**, *163*, 221.
(40) Narayanaswamy, R.; Ahmad, M. *Anal. Chim. Acta* **1994**, *291*, 255.
(41) Narayanaswamy, R.; Ahmad, M. *Talanta* **1995**, *42*, 1337−1344.
(42) Mansfeld, F. *Corrosion Mechanisms*; Marcel Dekker: New York, 1987; pp 265−270.
(43) Baes, C. F.; Mesmer, R. E. *The Hydrolysis of Cations*; John Wiley: New York, 1976.
(44) Allouche, Huguenard, C.; Taulelle, F. *J. Phys. Chem. Solids* **2001**, *62*, 1525.
(45) Benezeth, P.; Palmer, D. A.; Wesolowski, D. J. *Geothermics* **1997**, *26*, 465.
(46) Wesolowski, D. J.; Palmer, D. A. *Geochim. Cosmochim. Acta* **1994**, *58*, 2947.
(47) Cathalifaud, G.; Ayele, J.; Mazet, M. *Water Res.* **1997**, *31* (4), 689−698.

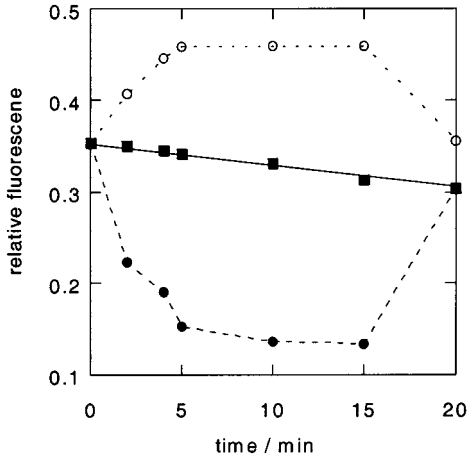

Figure 1. Change of the relative fluorescence intensity with time monitored with an imaging fiber modified with SNAFL-SE (λ_{ex} = 490 nm, λ_{em} = 540/650 nm) over an aluminum surface (filled circles) and over copper (open circles), E_{app} = 0.4 V/Cu, 0.1 M NaCl/buffer, pH 7; change at open circuit potential over aluminum (squares). Starting point corresponds to pH 7. After 15 min. the applied potential was switched off and the fluorescence returned to open circuit level.

in intensity corresponds to a decrease in pH. A vigorous acidification of the NaCl solution adjacent to the aluminum surface was observed (filled circles) that is due to dissolution of the aluminum portion of the wire corresponding to reactions 1 and 2. The pH close to the surface dropped from its bulk pH of 7.0 to 6.1. After 15 min, the applied potential was terminated, anodic dissolution stopped, and the pH returned to the solution pH of 7.0.

When the same fiber was brought into contact with the copper wire, the mean fluorescence increased spontaneously due to hydroxide ion production (reactions 3 and 4, open circles). This signal was reversible and returned to its initial value once the potential was removed, e.g., the pH dropped from about 9.5 (the fluorescence intensity was slightly outside the fiber's linear range) to 7.0. This result shows that the pH-sensitive fiber is able to distinguish between the base-generating cathode and the acid-generating anode. When the cell was left at its open circuit potential and no external potential was applied (Figure 1, squares), the acidification process over the aluminum surface was much slower as evidenced by only a small drop in fluorescence intensity with time.

To investigate the entire aluminum surface (1.5-mm diameter), the pH-sensitive fiber (350-μm diameter) was connected to a micromanipulator and 13 different regions on the aluminum surface were observed. Figure 2 shows the experimental setup. The imaging fiber was kept 10 μm above the aluminum surface, and the height was kept constant throughout the experiment. The fiber was placed in the middle of the surface, and a potential was applied between aluminum and copper. Every 10 min, the fiber was moved along the points of the grid as drawn on the aluminum surface in Figure 3. Scanning of these 13 points took 1 min. Figure 3 shows the change of pH at the 13 different sites on the aluminum wire in a pH 7.0 buffer NaCl solution monitored with the optical fiber. Before use, the pH-sensitive imaging fiber bundle was calibrated by measuring the average fluorescence intensity ratios in solutions of known pH. The pH of the rapidly acidified area dropped steadily for the first 10−20 min of exposure to the corrosion solution. After acidification, passivation of this region

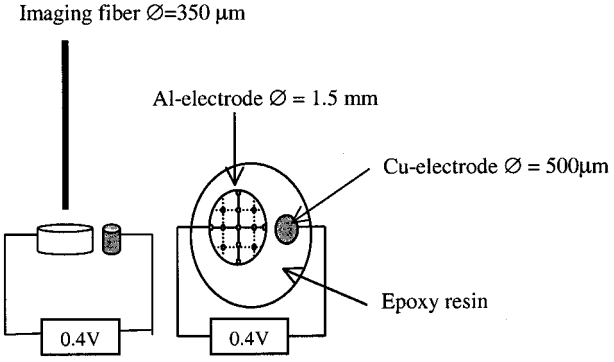

Figure 2. Experimental setup for scanning the aluminum surface.

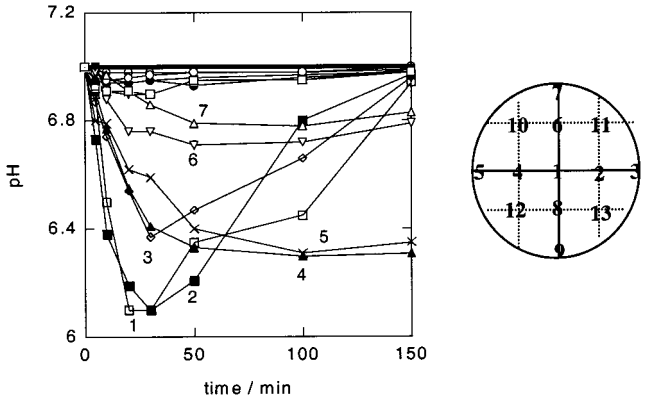

Figure 3. Change of pH with time monitored with an imaging fiber modified with SNAFL-SE (λ_{ex} = 490 nm, λ_{em} = 540/650 nm) over 13 different sites on an aluminum surface, 0.1 M NaCl/buffer, pH 7, E_{app} = 0.4 V/Cu; position 1 (open diamond), 2 (open circle), 3 (open square), 4 (full circle), 5 (full triangle), 6 (full diamond), 7 (full square), 8 (open triangle), 9 (open reverse triangle), 10 (cross), 11(full rev.triangle), 12 (circle), and 13 (square).

occurred and the pH returned to the buffer value of 7.0. Figure 3 shows that, on an aluminum surface of 7.0 mm^2, seven local corrosion sites could be observed and monitored with the fiber. The number of corrosion sites depended on the roughness of the aluminum surface and varied between 6 and 10 sites measured on different polished aluminum surfaces. Figure 3 also shows that, after 150 min, some corrosion sites were still active and had not passivated completely. The pH pattern observed on different areas of the metal is in accordance with the reaction mechanism in eqs 1−4.

Visualization of active corrosion sites on the aluminum surface was achieved by employing the optical fiber's imaging and chemical sensing capabilities. Figure 4 shows the images acquired on aluminum through an optical fiber imaging bundle modified with a layer of PAN/SNAFL-SE in 0.1 M NaCl/buffer solution containing 0.2% glycerin. Glycerin increases the viscosity of the solution and decreases the diffusion rate of the released protons. The fiber bundle was placed 10 μm over the aluminum without being moved during the experiments; i.e., the aluminum surface was not scanned in this case. Instead of monitoring the average fluorescence change over the fiber surface as in Figure 3, the imaging properties of the fiber were used to visualize in situ corrosion sites on the fiber, seen as darker regions in the images. Before corrosion was initiated, by applying an anodic potential between the aluminum and copper wires (corresponding to the image at t = 0 min), the fluorescence intensity of the pH-sensitive

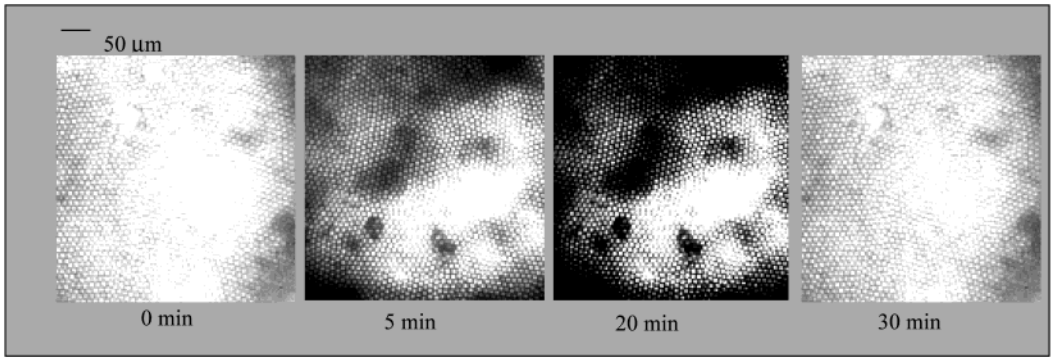

Figure 4. Change of fluorescence intensity with time monitored with an imaging fiber modified with SNAFL-SE (λ_{ex} = 490 nm, λ_{em} = 540 nm) over one region of an aluminum surface, 0.1 M NaCl/buffer +0.2% glycerin, pH 7, E_{app} = 0.4 V/Cu.

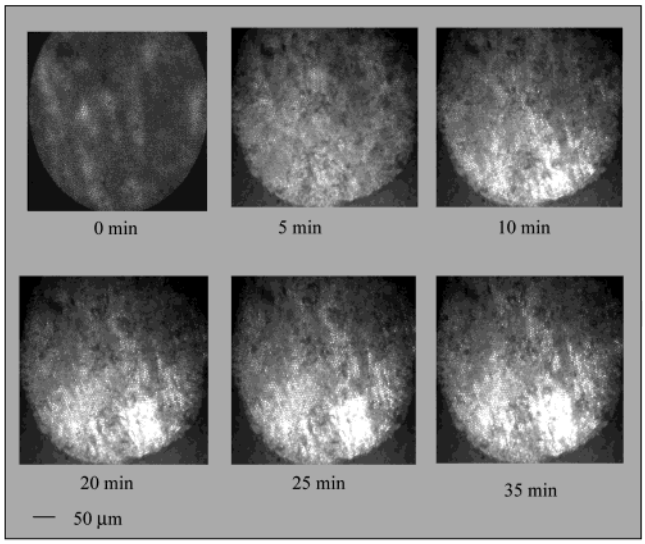

Figure 5. Change of the relative fluorescence intensity with time monitored with an unmodified imaging fiber at an aluminum surface with morin in solution, E_{app} = 0.4 V/Cu, 0.1 M NaCl/buffer, pH 7, + morin (10 mM), λ_{ex} = 430 nm, λ_{em} = 500 nm.

fiber over the aluminum surface was spread evenly. The images acquired after 5 and 20 min show areas of lower pH, seen as darker regions in the images. After about 30 min, the aluminum surface returned to its initial higher fluorescence levels suggesting passivation of the acidified regions according to the reaction mechanism outlined in eqs 1−4. By counting the number of pixels of the smallest dark region at ~7 o'clock in the figure, coupled with the 10 ± 2 μm distance from the surface, we estimate that the corrosion site must be less than 1 μm in diameter.

Morin in Solution. Morin (10 mM) was added to 0.1 M NaCl solution to observe the development of corrosion directly on the surface. An image of the surface was obtained with an unmodified imaging fiber, where the distal end was placed over the aluminum surface. The fiber was not moved and fluorescence images were recorded for 150 min. Figure 5 shows clearly that both the intensity and the area of fluorescence were increasing with time, corresponding to the formation of an aluminum complex of morin due to dissolution of the surface. This finding is in agreement with the observation by Smyrl,[19,20] who showed that the use of a fluorescence dye offers valuable insight into the corrosion process on aluminum alloys. In this experiment, we demonstrate that fluorescence sites are associated with localized dissolution of aluminum due to corrosion. In this approach, the fluorescence changes can be monitored over time and this enables us to follow the kinetics of corrosion in situ. Corrosion is extremely vigorous at the interface between aluminum and the epoxy resin and proximal to the copper surface. The spreading of the fluorescent area is a consequence of differences in pH between the surface and the bulk solution. Al^{3+} species are soluble in low-pH environments, diffuse into the bulk, where the pH is 7.0, and precipitate. In this way, the fluorescent area around the corrosion site grows with time, due to diffusion of the aluminum−morin complex away from the site.

Morin Bound to the Distal End of the Imaging Fiber. For determining the local aluminum ion concentration during dissolution, an Al^{3+}-selective imaging fiber sensor was developed. The distal end of a silanized imaging fiber was coated with an acrylamide-based polymer, PAN, to which morin was covalently bound through its hydroxyl group via a chemical cross-linker, cyanuric chloride.

Figure 6A shows the responses of the morin-based sensor to different aluminum ion concentrations in solution. For an Al^{3+} concentration of 30 mM, saturation was reached after 5 min. Such saturation behavior occurs because the total number of immobilized morin molecules is much less than the number of aluminum ions in the solution.[38] The concentration at which leveling off is observed depends on the number of morin sites available to bind to aluminum. A kinetic approach (Figure 6A) was therefore used to quantify the aluminum concentration in which the fluorescence signal was measured after a fixed constant time. In this work, the time was fixed at 5 min. Figure 6B plots the relative fluorescence intensities extracted from Figure 6A for different aluminum ion concentrations after the fiber had been dipped in solution for 5 min. The fluorescence response kinetics of the immobilized morin sensor increased with increasing Al^{3+} concentration and had a linear concentration range of Al^{3+} between 0.5 and 5.0 mM. Above 5.0 mM, there was a change in slope and the response leveled off due to saturation. After each measurement, the fiber was regenerated by stripping the aluminum from the fiber with EDTA (a stronger chelating agent than morin) and then rinsing with water and buffer. After about 100 measurements, the fiber still responded to different aluminum ion additions. When not in use, the fiber was stored in buffer solution away from light to minimize photobleaching of the dye. This metal-sensitive fiber was used to measure the release of Al^{3+} during aluminum

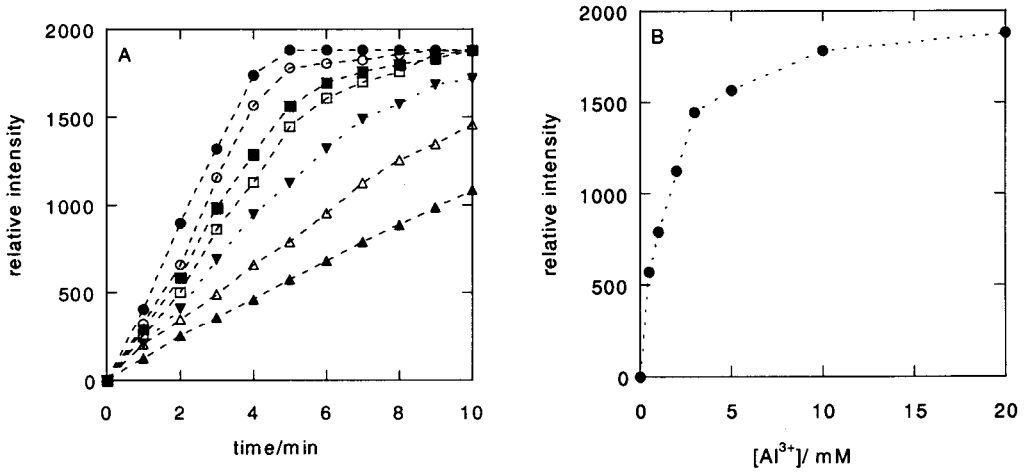

Figure 6. Response curves and resulting calibration curve for aluminum ion in phosphate buffer solution, pH 7, using an imaging fiber with covalently bound morin (λ_{ex} = 430 nm, λ_{em} = 500 nm), (A) Kinetic plots for different Al^{3+} concentrations 30 (full circle), 20 (open circle), 10 (full square), 5 (open square), 2 (full reverse triangle), 1 (open triangle), and 0.5 mM (full triangle), (B) Calibration curve for Al^{3+} obtained by reading off the relative intensities of (A) after 5-min acquisition time.

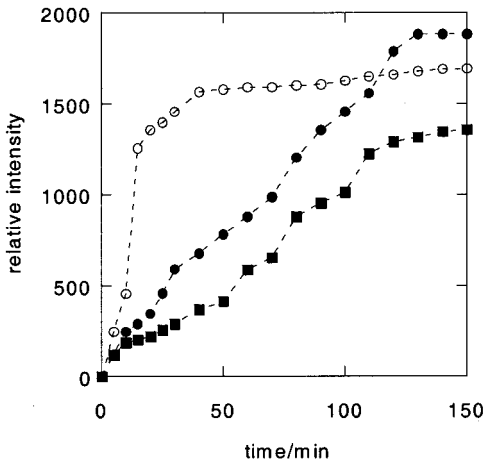

Figure 7. Change of the relative fluorescence intensity with time during three different experiments monitored with an imaging fiber with covalently bound morin at an aluminum surface, E_{app} = 0.4 V/Cu, 0.1 M NaCl/buffer, pH 7, λ_{ex} = 430 nm, λ_{em} = 500 nm, 1 experiment (full circle), 2 experiment (open circle), 3 experiment (full squares).

dissolution (reaction 1), the first step in the surface corrosion process.

The Al^{3+}-sensitive optical fiber bundle was placed over different areas in three separate experiments on the aluminum surface, and the release of Al^{3+} was investigated. Different behaviors were observed. In the first experiment (Figure 7, full circles), the release of aluminum ions could be observed for longer than 120 min and the signal went to saturation at longer times. In contrast to this experiment, the other two experiments exhibited an increase in aluminum concentration with time, but before saturation was reached, the aluminum ion release stopped and no further increase in fluorescence signal was observed. The termination of Al^{3+} release is a consequence of corrosion site passivation. Quantitative information cannot be obtained directly because of the irreversibility of the fiber and its saturation behavior; however, several general conclusions can be drawn. The average amount of Al^{3+} released during dissolution as monitored with the fiber (Figure 7) varies considerably. The experiment shown as open circles in Figure 7 corresponds to a release that generates an average local concentration at the fiber of less than 0.5 mM after 5 min while the other two experiments show an average release that is much lower. These differences in release profiles may be due to different surface roughnesses or differences in the sizes of the active sites. Furthermore, as the concentration of Al^{3+} ions is dependent on the solution pH, slightly more acidic conditions may result in higher measured aluminum concentrations.[47] Since morin is covalently linked to the polymer, no leakage of the dye onto the surface was observed. This result was confirmed by removing the solution after the experiment and scanning the aluminum surface with an unmodified imaging fiber. No fluorescence signals were found.

Cerium Chloride. Cerium chloride was used to study its inhibition effect on the corrosion of aluminum in neutral salt solution. Cerium chloride is a cathodic inhibitor limiting the reduction of oxygen and thus reducing the current supply to the anode. Hinton[32−34] and co-workers were the first to investigate the effect of $CeCl_3$ on corrosion. They studied the protective effects toward aluminum when increasing concentrations of $CeCl_3$ were present in the NaCl solution and demonstrated that the corrosion rate decreased steeply and constantly from 0 to 100 ppm $CeCl_3$ and leveled off at higher concentrations of $CeCl_3$. We performed all the corrosion inhibition experiments in 0.1 M NaCl buffer solutions in the presence of 3.0 mM $CeCl_3$. This concentration corresponds to an inhibitor concentration of 735 ppm and is high enough to give stable and reproducible corrosion characteristics. The current dropped from 50 μA (determined after 1 min) in the noninhibited case to 20 μA in the presence of $CeCl_3$, indicating that this compound blocks oxygen reduction on the cathodic site. The decreased current drop reflects the reduced dissolution on the anodic site due to the presence of the inhibitor.

First, the pH-sensitive imaging fiber was placed over the aluminum surface and the change of pH was determined over time by monitoring the relative fluorescence intensity in the presence of $CeCl_3$ (Figure 8A). The fiber was scanned over the surface, as described above, and out of the 13 surface locations investigated, three showed aluminum dissolution behavior. Acidification occurred in the first 30 min after a potential of 0.4 V/Cu

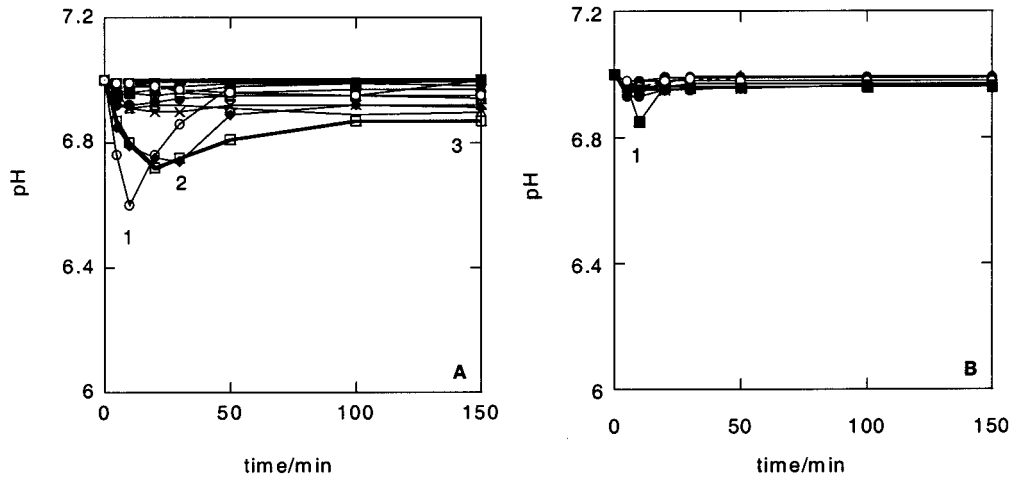

Figure 8. Change of pH with time monitored with an imaging fiber modified with SNAFL-SE (λ_{ex} = 490 nm, λ_{em} = 540/650 nm) over different sites on an aluminum surface, E_{app} = 0.4 V/Cu, 0.1 M NaCl/buffer, pH 7, + 10 mM $CeCl_3$ (A), 0.1 M NaCl/buffer, pH 7, + 10 mM 8HQ (B); position 1 (full route), 2 (open circle), 3 (open square), 4 (full circle), 5 (full triangle), 6 (full route), 7 (full square), 8 (open triangle), 9 (open reverse triangle), 10 (cross), 11 (full reverse triangle), 12 (circle), and 13 (square).

was applied. By comparing the fluorescence signals in the $CeCl_3$ case (Figure 8A) to the ones where only NaCl was present in solution (Figure 3, the same fiber was used for both experiments), the effect of $CeCl_3$ on the corrosion behavior can be seen clearly. When $CeCl_3$ was present, the number of corrosion sites over the aluminum surface was reduced by half and there was a reduction in the magnitude of the pH change close to the aluminum surface; in $CeCl_3$, there was only a 0.4 pH unit change compared to 0.9 in NaCl. After 150 min, all active sites were passivated in the presence of $CeCl_3$ whereas there were still some active sites in NaCl.

The decrease in current, the decrease of the amount of active sites on the aluminum surface, and the faster passivation are all clear indications that $CeCl_3$ is inhibiting corrosion effectively. The mechanism causing the reduction in the rate of the cathodic reaction sites in $CeCl_3$, is believed to be the result of precipitation of an insoluble film at these sites, which inhibits the mass transfer of oxygen to the surface.[30,48] This inhibition is associated with a drop in the current density, as observed in our experiments, due to deposition of a cerium-rich film on the copper surface as recently confirmed by Isaacs.[49−51] The hydroxyl groups that form over the cathodic copper site react with cerium ions present in the solution giving rise to cerium islands, thereby blocking the cathodic reaction site, decreasing the cathodic current available, and thus reducing the rate of corrosion.

In the NaCl case, the reductions of water and oxygen are taking place on the copper surface providing a total of six OH^-, with two OH^- coming from the reduction of water (reaction 3) and four OH^- coming from the reduction of oxygen (reaction 4). In the case of cathodic inhibition, the oxygen reduction is blocked (reaction 4), and instead of releasing six OH^- on the cathode, only two OH^- are released from the reduction of water (reaction 3), leading to a smaller basic pH cloud over the copper surface. The pH-sensitive imaging fiber was used to monitor the surface of the copper surface independently in the presence and absence of inhibitors (Figure 9). The demonstration that part of the cathodic reaction is blocked by cerium chloride is seen in the change of pH close to the copper surface in Figure 9 relative to NaCl. The initial pH of 7.0 is changed in the NaCl case to values as high as pH 9.5, while in $CeCl_3$ a smaller shift to pH 8.1 was seen. At the copper surface in the $CeCl_3$ solution, reaction 2 gets blocked after a time delay of ~5 min, due to the formation of an oxide layer on the copper surface.

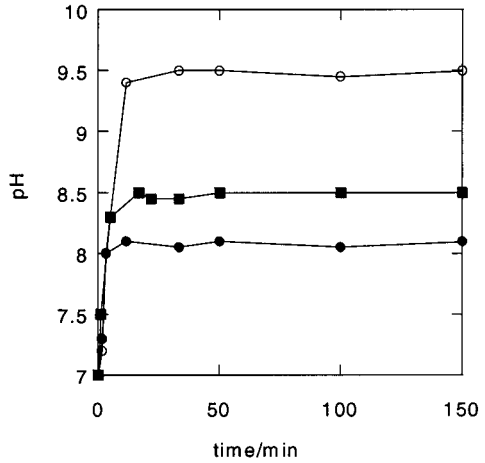

Figure 9. Change of pH with time monitored with an imaging fiber modified with SNAFL-SE (λ_{ex} = 490 nm, λ_{em} = 540/650 nm) over a copper surface, E_{app} = 0.4 V/Cu, 0.1 M NaCl/buffer, pH 7 (open circles), 0.1 M NaCl/buffer, pH 7, + 4 mM $CeCl_3$ (filled circles), and 0.1 M NaCl/buffer, pH 7, + 4 mM 8-HQ (squares).

To understand what was occurring at the aluminum surface, two studies were conducted. First, morin was added to the $CeCl_3$-containing NaCl solution. Figure 10A shows one of the images obtained with an unmodified fiber when the surface was scanned after a potential of 0.4 V had been applied between the aluminum and the copper wire. A detectable increase in fluorescent signal due to the formation of the aluminum−morin chelate was recorded after 30 min.

(48) Scully, J. C. *The Fundamentals of Corrosion*; Pergamon Press: New York, 1990; p 143.
(49) Aldykewicz, A. J.; Isaacs, H. S.; Davenport, A. J. *J. Electrochem. Soc.* **1995**, *142* (10), 3342.
(50) Aldykewicz, A. J.; Isaacs, H. S.; Davenport, A. J. *J. Electrochem. Soc.* **1996**, *143* (1), 147.
(51) Davenport, A. J.; Isaacs, H. S.; Kending M. W. *Corros. Sci.* **1991**, *32* (5−6), 653.

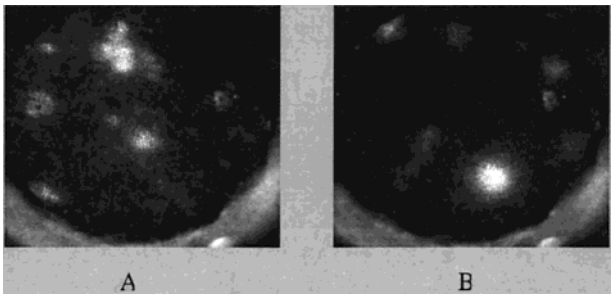

Figure 10. Change of relative fluorescence intensity with time monitored with an unmodified imaging fiber at an aluminum surface, E_{app} = 0.4 V/Cu, 0.1 M NaCl/buffer, pH 7, + morin (10 mM) + 3 mM $CeCl_3$ (A) and 0.1 M NaCl/buffer, pH 7, + morin (10 mM) + 3 mM 8-HQ (B); λ_{ex} = 430 nm, λ_{em} = 500 nm.

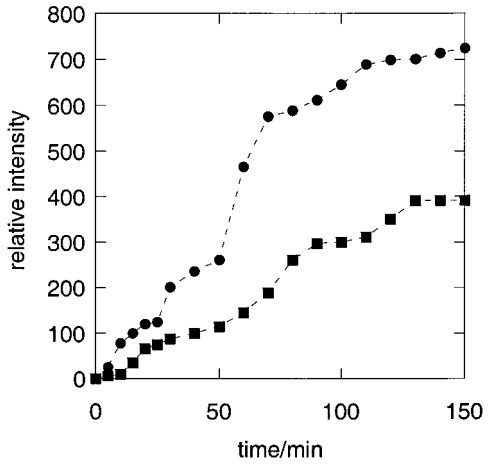

Figure 11. Change of concentration of aluminum over time monitored with a morin-modified imaging fiber at an aluminum surface, E_{app} = 0.4V/Cu, 0.1 M NaCl/buffer, pH 7, + 3 mM $CeCl_3$ (circles) and 0.1 M NaCl/buffer, pH 7, + 3 mM 8-HQ (squares); λ_{ex} = 430 nm, λ_{em} = 500 nm.

In a second experiment, a morin-modified optical fiber was used to obtain information about the relative concentration range of aluminum ions released during aluminum dissolution at different areas of the surface in the presence of $CeCl_3$ (Figure 11, circles). In four cases (data not shown), no change in fluorescence signal was observed, indicating that the fiber was placed over a part of the aluminum surface where no corrosion process had been initiated. From the one spot where aluminum dissolution could be monitored, the maximum relative fluorescence of 715 corresponds to an Al^{3+} release rate (determined from Figure 6B) that is one-tenth the rate of corrosion in NaCl as determined by comparing the relative fluorescence after 120 min with the calibration curve in Figure 6B.

8-Hydroxyquinoline. Using cerium chloride, the resistance of aluminum against corrosion can be attributed to a rapidly formed oxide film on the copper surface. A number of organic compounds have also been described as aluminum corrosion inhibitors, the majority being nitrogen-containing compounds.[52−55] We investigated the effectiveness of 8-hydroxyquinoline (8-HQ) as a corrosion inhibitor for aluminum. The concentration of 8-HQ tested was 3.0 mM in buffer, which is close to its solubility limit. Figure 8B shows the change of pH over time when a pH-sensitive imaging fiber was placed over the aluminum surface. As in the case of NaCl and $CeCl_3$, 13 spots were examined by scanning the fiber at constant height over the surface. The number of active sites was drastically diminished in the presence of 8-HQ, with only one aluminum dissolution recorded. Acidification also proved to be less vigorous as seen in a change of 0.15 pH unit, compared to 0.4 and 0.9 for $CeCl_3$ and NaCl, respectively, and only occurred for the first 20 min. After 20 min, the active site was passivated.

The aluminum surface was investigated by chemical imaging using morin in solution. Figure 10B shows the image obtained of the aluminum surface in the presence of 8-HQ after a potential was applied for 150 min. The fluorescence signal looks very similar to $CeCl_3$. Only one strong fluorescent spot could be detected, showing a circular shape. No spreading of fluorescence was observed with time as in NaCl solution. From the literature, it has been shown that $CeCl_3$ inhibits the cathodic reaction during galvanostatic corrosion[48−51] by forming cerium islands over the copper and thereby blocking the cathodic reaction site. We confirmed this mechanism by monitoring the pH change over the copper surface with the pH-sensitive imaging fiber (Figure 9). The change in pH was less drastic than in a pure NaCl solution because the oxygen reduction was blocked (reaction 4) causing only two OH^- to be released from the reduction of water on the cathode (reaction 3) instead of six OH^-. The pH-sensitive imaging fiber was also used to monitor the copper surface independently in the presence and absence of inhibitors (Figure 9). In comparison to the small pH effects on the cathodic reaction site in the presence of $CeCl_3$, the change of pH with 8-HQ in solution was larger but still less severe than in NaCl solution. This result points toward different reaction mechanisms of the inhibitors. While $CeCl_3$ blocks the cathodic oxygen reduction effectively, only a partial limitation of oxygen reduction on the copper surface is seen for 8-HQ. The main process of inhibition in the 8-HQ case seems to be adsorption of the 8-HQ on the aluminum anode, which slows down the corrosion rate and prevents adsorption of chloride ion and thus the destruction of the aluminum oxide layer. It is possible that an insoluble chelate of aluminum, $Al^{3+}(8\text{-}Q^-)_3$, may be formed, which competes with the formation of the insulating aluminum hydroxide (reactions 2a−e).[29] Similar behavior was found by Garrigues,[29] who observed a strong modification of the cathodic current intensity when aluminum was immersed over longer times in a sodium chloride solution containing 8-HQ. Such a change would not occur with an adsorption layer only on the anode but must also result in the formation of a protective film on the copper surface. The more basic pH measured in these experiments seems to be further evidence for this mechanism. The current dropped to 30 μA after 1 min (compared to 50 μA in NaCl and 20 μA in $CeCl_3$), providing additional evidence that a thin film blocks the cathodic side. The increase in fluorescence when the Al^{3+}-sensitive morin-based optical fiber was placed over the aluminum electrode in the presence of 8-HQ is seen in Figure 11 (squares). As with $CeCl_3$, in most cases, no fluorescence change could be observed. After 30 min, no further increase in fluorescence was observed. In the single case where a fluorescence increase could be observed, the amount of aluminum dissolved in the presence of

(52) Metikos-Hukovic, M.; Babic, R.; Grubac, Z.; Brinic, S. J. *Appl. Electrochem.* **1994**, *24*, 772.
(53) Leidheiser H.; Konno, H. *J. Electrochem. Soc.* **1983**, *30*, 747.
(54) Tribonod, F.; Fiaud, C. *Corros. Sci.* **1978**, *18*, 139.
(55) Niki, K.; Delnick, F. M.; Hackerman, N. *J. Electrochem. Soc.* **1975**, *122*, 855.

8-HQ was 25% lower than that observed for $CeCl_3$. This result is in agreement with the adsorption mechanism explained above. 8-HQ is adsorbed and prevents the reaction of chloride ions and the destruction of the aluminum oxide layer. 8-HQ is a more efficient corrosion inhibitor for aluminum, which was experimentally verified by the number of active sites on the aluminum surface and the amount of aluminum released during the aluminum dissolution process.

CONCLUSION

Optical fibers with different indicators on the distal tips were used to reveal both temporal and spatial details of the chemistry around individual reaction sites. The fiber-optic imaging sensors described here enable the initial stages of corrosion to be visualized and facilitate our understanding of the mechanism underlying corrosion on a molecular level. The corrosion behavior of a galvanic aluminum/copper couple was investigated in neutral NaCl solution using both pH- and metal-sensitive imaging fiber arrays. Real-time measurements were demonstrated of the local acidity/basicity produced over corrosion sites. The addition of the fluorescent dye morin, which forms a highly fluorescent chelate with Al^{3+}, helped identify specific chemical features occurring on the metal surfaces. Furthermore, the Al^{3+}-sensitive sensor helped to identify the heterogeneous reactions taking place at the aluminum surface by monitoring the release of aluminum with time in different corrosive solutions and in the presence of inhibitors. It is believed that cerium chloride inhibits corrosion by the formation of a cerium-rich film on the cathodic site. 8-HQ was found to prevent the adsorption of chloride ions and thus improves the corrosion resistance due to the formation of an insoluble chelate of aluminum which protects the oxide film while forming a thin cathodic film as well. Cerium chloride was less effective, however, in preventing aluminum dissolution than was 8-HQ. The advantage of the covalent attachment of dyes to fibers is that these studies could be conducted without the addition of any soluble indicators to the solution, which could perturb the results. The approach is, however, not a truly nonperturbing one, as we have a sensor over the surface. As a consequence, the metal surface of interest is not freely exposed to the surrounding solution. One of the limitations of this approach is the irreversible response of the Al^{3+} sensors due to the formation of a chelate between the functional groups of the dye and the analyte. The spatial resolution of the pH- and metal ion-sensitive fibers is in the micrometer range as it is dependent on the diameter of the fibers (4 μm in the present case). To obtain nanometer resolution, obtainable by other optical methods, the diameter of the each fiber in the bundle must be reduced. Research in this direction is currently being undertaken in our laboratory.

ACKNOWLEDGMENT

The authors thank Dr. Caroline L. Schauer for helpful discussions on fibers and dyes and the National Institutes of Health for financial support.

Received for review July 23, 2001. Accepted November 19, 2001.

AC0108257